PHYSICAL REVIEW B VOLUME 25, NUMBER 4 15 FEBRUARY 1982

Tight-binding calculations for the electronic structure of isolated vacancies and impurities in III-V compound semiconductors

D. N. Talwar* and C. S. Ting
Department of Physics, University of Houston, Central Campus, Houston, Texas 77004
(Received 22 June 1981)

In the second-neighbor tight-binding framework and using the well-known $\vec{k}$-space Green's-function approach, we have calculated the energies of deep highly localized electronic states due to isolated vacancies and simple point defects in III-V compound semiconductors. Using existing pseudopotential data for the band structures, we are able to calculate 21 (out of 23) interaction integrals with the help of the least-squares-fitting technique. The Green's functions in the a_1 (s-type) and t_2 (p-type) symmetries have been numerically evaluated by using the eigenfunctions and eigenvalues of the host systems. The calculated results are discussed and compared with the existing theoretical and experimental data. The pinning energies of the anion vacancy levels of t_2 symmetry are found to be almost the same for Ga-In pnictides while they are different for the Ga-Al and In-Al compounds. No such correlation of pinning energies due to cation vacancies has been noticed. These results provide justification to the recent experimental speculations that the anion vacancies near the surface are responsible for determining the position of the Fermi level. This also lends support to the speculation that, similar to $Ga_{1-x}In_xAs(P)$ ternaries, the Fermi-level variation for the GaSb-InSb system should be independent of the composition factor.

I. INTRODUCTION

The study of unoccupied deep impurity states in the critical band gap of elemental and compound semiconductors provides information for various technologically important properties in solid-state devices.[1–4] The experimental data for such impurity states are either incomplete or contradictory.[1] Deep-level transient spectroscopy (DLTS) and the methods which measure absorption or emission provide information for the energy of the defect state while the impurity which causes such state is not completely identified. From the variation of some of the physical properties with the impurity concentration, most of the observations of the deep levels can be correlated with the isolated defects.[1] This is, however, not always a very convincing identification as the dopant may generate intrinsic lattice defects and can form various complexes. It is therefore essential to identify the defects which cause deep traps before measures can be devised to control their concentration in the technology of electron transfer devices (e.g., light-emitting diodes etc.). Since the existing experimental data is either insufficient or sparse, theoretical calculations are also equally important. Despite the numerous theoretical investigations of solving the Hamiltonian representing an impurity potential using various approximations, the electronic structure of deep defect states in semiconductors is still an unsolved problem. However, the use of the pseudoimpurity and the self-consistent model potential calculations in recent years have provided means for considerable progress to understand the subject by performing realistic calculations. An excellent critical survey of the methods presently available to the theorists on the subject has been provided by Pantelides[3] and more recently by Jaros.[4]

Two types of important calculations have emerged with the same basic idea in common:

(a) The molecular-cluster approach, which offers a relatively faster and less complicated scheme, has been applied to the electronic states of isolated vacancies and substitutional impurities.[5–8] In this method the impurity atom is considered to be surrounded by a limited number of host-lattice atoms and the remaining solid enters the problem via the boundary conditions on the cluster wave functions. The method, within its own limitations, has been claimed to provide promising results. However, it has been pointed out by Messmer *et al.*[9] that the size of the cluster and the choice of the boundary conditions can affect the existence of the localized states. Moreover, the calculations do not always

provide a reliable starting point both for the perfect and the imperfect clusters especially for many-valley direct-gap materials[4] (e.g., GaAs and ZnSe). In Sec. III we will show that the results based on a cluster of seventeen atoms[8] for vacancy levels in GaAs are at variance with the most recent self-consistent,[10] as well as semiempirical calculations.

(b) The second category of methods for localized perturbations that has gained momentum with the advent of high-speed computers, involved with the detailed electronic structure of the host systems.[10–21] The well known Green's-function method in the Wannier representation, proposed long ago by Koster and Slater,[22] was first numerically implemented by Callaway[11] and co-workers for an isolated vacancy and divacancy in Si. In this representation, although the elements of the Green's-function matrix have rather simplified forms, there arises complexities and ambiguities in defining the perturbation (as the size of matrix depends both on the number of bands and the number of sites over which the impurity potential extends). Starting from the band structure of Si and considering the impurity potential to be negative of the atomic pseudopotential for an isolated vacancy, Callaway and Hughes[11] have made extremely difficult calculations in the Wannier representation. By including even the maximum number of bands and sites in the numerical calculations, it is worth mentioning that no bound state in the gap has been obtained for Si vacancy. However, if the vacancy potential is made stronger by a factor of 1.1 (than the negative atomic potential) a vacancy state of a_1 symmetry appears in the band gap. This result is rather difficult to interpret on the basis of physical arguments primarily because a_1 level (being spherically symmetric) can not account for the observed Jahn-Teller distortion in Si. Secondly, a larger repulsive potential should have extracted first a t_2 level rather than a_1 from the top of the valence band which has a strong t_2 character.

While analyzing the calculations of Callaway *et al.*[11] for a given vacancy potential, Pantelides[3] has realized that their results are not convergent. Moreover, a dramatic change occurs in the bound-state energies if additional bands and sites are included. Although the Si vacancy levels are not well determined experimentally, they are believed to be deep (few tenths of an eV) in the forbidden gap.[19–20] Again from the electron paramagnetic resonance (EPR) measurements, it has been found that both the singly positive (V^+) and negative (V^-) charged states of Si vacancy undergo a structural reconstruction.[7] Although the work of Callaway and co-workers,[11] did not provide conclusive answers to the observed experimental facts, it nevertheless represented the first major achievement in the application of the Koster-Slater method to real solids.

A significant contribution to generalize the Slater-Koster method in terms of a localized basis set, rather than Wannier functions as a basis, was provided by Lannoo and Lenglart.[23] Starting from a simplified model in the nearest-neighbor approximation with s and p orbitals on each atom and using linear combination of atomic orbitals (LCAO), Lannoo and Lenglart performed band-structure calculations for neutral vacancy is diamond. The Hamiltonian matrix elements are treated as free parameters to obtain the approximate representation of the band structure. The unrelaxed vacancy is defined by removing an atom (i.e., removing all the interactions with the neighboring atoms of various orders) from a lattice site and considering the positions of all other atoms to be unchanged. In this picture the vacancy exhibits an extreme case of infinite defect potential (see Ref. 14 for a complete discussion). In the Green's-function framework, it is straightforward to show that the impurity states of a_1 (or s) and t_2 (or p) symmetry can be obtained by $\langle s \mid G^0(E) \mid s \rangle = 0$ and $\langle p \mid G^0(E) \mid p \rangle = 0$, respectively. Bernholc and Pantelides[14] have calculated the Green's function and thereby the vacancy levels in Si, Ge, and GaAs by incorporating the Slater-Koster parametrization of Pandey and Phillips.[24] For neutral Si vacancy, the simplified semiempirical calculation has provided a bound state of t_2 symmetry (0.27 eV above the valence-band edge). Self-consistent calculations performed in recent years have also confirmed the occurrence of a t_2 state but the position of the bound level above the valence band is found to be at 0.76,[19] 0.7,[20] or 0.5 eV.[18] The discrepancy, in the semiempirical calculation,[14] has been speculated[17] as being due to the poor description of the conduction bands in the second-neighbor parameterization of Pandey and Phillips.[24]

Quite recently Krieger and Laufer[25] have examined the dependence of the vacancy states on the choice of the localized basis functions in the tight-binding method. They believe that if Wannier functions are employed as a basis, no ideal vacancy gap state will exist—a result which has already been discussed in length by Callaway.[11] On the

other hand, if the atomic orbitals are taken as a basis, no vacancy state will appear in the limit when the number of orbitals on the atom to be removed approaches infinity. In the finite band model, however, there exists the possibility of the occurrence of gap states.

Here, it is fair to mention that the Green's-function method in the localized-basis (sp^3) representation is not completely inadequate and it at least provides qualitative information which is of course, complementary to (and cannot replace) the most sophisticated calculations aimed for the accurate determination of the deep levels in semiconductors.[10,18–21] Despite the problems to precisely account for the perturbation, the substantial advantage of this technique over other methods is that in terms of realistic Hamiltonians one can address not only the change in the bulk properties induced by the point defects, but, in principle, can extend it to understand the properties of surfaces, interfaces in the hetrojunction overlayers, and super lattices (see Ref. 26 for further discussions).

In a subsequent study, Jaros[12] has also realized the significance of localized-basis instead of Wannier functions but using the energy spectrum from pseudopotential method. Although the energy spectrum and the wave functions of an unperturbed crystal can adequately be represented using the empirical pseudopotential, the method suffers from a number of shortcomings with respect to its implementation to the impurity problem—especially with the distribution of the electron density near the defect, the effective charges of the atoms, the spin-density distribution, and the hyperfine fields at the nuclei. Again, the type of calculations which Jaros[12] has presented require considerable amount of computational work and there still remains an ambiguity with respect to the selection of the model potential parameters see Jaros and Srivastva in Ref. 12(b) and Srivastva in Ref. 12 (c).

The purpose of the present work is the show that an orthogonal basis of tight-binding parametrization obtained for III-V compounds when incorporated in the Green's-function framework might be useful for understanding the vacancy states and can be helpful for predicting the positions of the substitutional impurity levels. Unlike the existing tight-binding calculations,[27–30] we will show that the Slater-Koster Hamiltonians with interaction integrals up to and including second neighbors, obtained from the least-squares fitting method, not only provide good fit to the pseudopotential band structures[31–33] but also produce fairly accurately the band gap as well as the conduction bands. An elaborate representation of the band structures with interactions beyond the second neighbors will not be useful at this time owing to the insufficient pseudopotential data (cf. appendix). For neutral vacancy levels in GaAs and GaP, our results are in very good agreement with the most recent self-consistent calculations.[10,21] Similar calculations have been performed for other III-V compounds.

This work is also motivated by efforts made in recent years to understand the basic mechanisms that control the formation and the operation of the Schöttky-barrier behavior observed for a large range of metals on clean III-V semiconductors.[34–37] Chye *et al.*[34] have proposed a model where the Fermi level at the interface is considered to be pinned by defects such as vacancies and vacancy clusters and this has received considerable support by various experiments on vacuum-cleaved surfaces of III-V semiconductors.[34–36] More recently, the variation of the surface Fermi level in mixed [$Ga_{1-x}In_xAs(P)$ and $Ga_{1-x}Al_xAs$] systems has also been reported as a function of alloy composition.[35,36] For Ga-In pnictides, the Fermi-level position is found to be independent of the composition, while for ternary alloys involving aluminium, it varies linearly with the Al content. Theoretically, the highest occupied level in the netural anion vacancy on the (110) surface has been very well correlated with the observed Fermi-level variation.[37] Moreover, it has been speculated by Keuch and McCaldin[36] that similar to $Ga_{1-x}In_xAs(P)$ systems, the Fermi-level pinning in $Ga_{1-x}In_xSb$ system should also be independent of the concentration. Since the same trend is exhibited for the highest occupied neutral-anion-vacancy level on the (110) surface[37] and in the bulk, our results for the isolated anion and cation vacancies may be useful to understand the experiments and to provide some clues in favor of the proposed model for correlating the effect of anion vacancies with the Fermi-level pinning (cf. Sec. III).

The paper is organized into four sections. To understand the electronic properties of point defects, especially the isolated vacancies, we have outlined the Green's-function method in the tight-binding framework in Sec. II. The calculated results for the isolated vacancies and deep impurity levels have been discussed and compared (in Sec. III) with the existing experimental and theoretical data. The concluding remarks are presented in Sec. IV.

II. THEORETICAL CONSIDERATIONS

A. Tight-binding or LCAO method for the band structure

The method of solving the Schrödinger equation for a multiatomic system by expanding the eigenfunctions of the effective one-electron Hamiltonian in a sum of atomic orbitals is called the linear combination of atomic orbitals (LCAO). The technique traditionally developed for molecular systems in *quantum chemistry* has been applied for a variety of electronic properties of tetrahedral semiconductors. In this method the one-electron wave functions $\psi_v(\vec{r})$ of the polyatomic system, are expanded in atomic like basis functions $\phi_\alpha(\vec{r})$ centered on atomic positions $\vec{R}_j$ as[39]:

$$\psi_v(\vec{r})=\sum_{\alpha j} A^v_{\alpha j}\phi_\alpha(\vec{r}-\vec{R}_j)\ , \tag{1a}$$

or equivalently,

$$\psi_v(\vec{r})=\sum_{\alpha j} A^v_{\alpha j}\phi_{\alpha j}(\vec{r})\ . \tag{1b}$$

Using variational method, the energy can be minimized by varying the coefficients of A's and this provides the equation:

$$\sum_{\alpha' j'}[H^0_{\alpha\alpha'}(\vec{R}_j-\vec{R}_{j'}) -E_v S_{\alpha\alpha'}(\vec{R}_j-\vec{R}_{j'})]A^v_{\alpha' j'}=0\ , \tag{2}$$

where H^0 is the one-electron Hamiltonian of the system,

$$H^0_{\alpha\alpha'}(\vec{R}_j-\vec{R}_{j'})=\langle\phi_{\alpha j}\,|\,H^0\,|\,\phi_{\alpha' j'}\rangle\ ,$$

and

$$S_{\alpha\alpha'}(\vec{R}_j-\vec{R}_{j'})=\langle\phi_{\alpha j}\,|\,\phi_{\alpha' j'}\rangle\ .$$

The solution of the multicenter nature of the problem requires several approximations. In the Hückel method, for example, $H^0_{\alpha\alpha'}(\vec{R}_j-\vec{R}_{j'})$ is assumed to be proportional to $S_{\alpha\alpha'}(\vec{R}_j-\vec{R}_{j'})$ for $j\neq j'$. For small values of the overlap integrals, the above approximation is justified and we refer to the work of Fischer-Hjalmars[40] for further discussion.

In the above-mentioned molecular picture, the LCAO method can be applied to real solids as well. For the perfect tetrahedral semiconductors, the periodicity allows to introduce a wave vector $\vec{k}$ and one can construct *two* Bloch functions centered on the *two* atoms in the unit cell. For zinc-blende-type crystals we define the Bloch sums:

$$b^{\alpha v}_{\vec{k}}(\vec{r})=\frac{1}{\sqrt{N}}\sum_j \exp\{i[\vec{k}\cdot(\vec{R}_j+\vec{\tau}_v)]\} \times\phi_{\alpha j}(\vec{r}-\vec{\tau}_v)\ . \tag{3}$$

Here, the atomic orbitals $\phi_\alpha(\vec{r}-\vec{R}_j)$ [or $\phi_{\alpha j}(\vec{r})$] are considered to be centered at the anion site [supposed to be at the origin] and the orbitals $[\phi_{\alpha j}(\vec{r}-\vec{\tau}_v)]$ centered at the cation site are supposed to be displaced by $\vec{\tau}_v=[1/4a\,(111)]$ from the anion. The term a is the edge length of the elementary cube of the face-centered cubic lattice and the label α corresponds to s, p_x, p_y, and p_z character of the atomic orbitals:

The Bloch functions are then expanded as Eq. (1):

$$\psi^0_{n\vec{k}}(\vec{r})=\sum_{\alpha v} A^n_{\alpha v}(\vec{k})b^{\alpha v}_{\vec{k}}(\vec{r})\ . \tag{4}$$

In terms of the orthogonal atomic orbitals, the diagonalization of the secular matrix $H^0(\vec{k})$ with elements $\langle b^{\alpha v}_{\vec{k}}\,|\,H^0\,|\,b^{\alpha' v'}_{\vec{k}}\rangle$ at each $\vec{k}$ will provide us with the eigen values $E_{n\vec{k}}$ and the corresponding eigenvectors $A^n_{\alpha v}(\vec{k})$. In the tight-binding framework, the elements $\langle\phi_{\alpha j v}\,|\,H^0\,|\,\phi_{\alpha' j' v'}\rangle$ which are considered to construct $\langle b^{\alpha v}_{\vec{k}}\,|\,H^0\,|\,b^{\alpha' v'}_{\vec{k}}\rangle$ are treated as free parameters.

In the LCAO method the basic problem is to find the Hamiltonian matrix elements between the various basis states. In the notations of Slater and Koster and following Dresselhaus and Dresselhaus[41] the matrix elements can be written between basis functions $(sp)^3$ considering various possible interactions. In the nearest-neighbor approximation, Chadi and Cohen[27] have reported the (8×8) secular determinant for zinc-blende-type crystals. In the appendix, we have constructed a nonzero symmetrized (8×8) Hamiltonian matrix with twenty-three two-center second-neighbor-interaction integrals, and have suggested the method for their numerical evaluation. For all the perfect III-V compounds studied here, our tight-binding parameters provide fairly accurately the valence bands, band gaps and reasonable conduction bands (cf. Sec. III).

B. Green's functions

In order to calculate the electronic properties of semiconductors with a localized defect potential we have to solve the Schrödinger equation[3]

$$H\psi=E\psi \tag{5}$$

for energy E and wave function ψ of an effective Hamiltonian H ($\equiv H^0+P$). The above equation can be recast in terms of Green's function as

$$\psi=G^0(E)P\psi\ , \tag{6}$$

or explicitly

$$[I-G^0(E)P]\psi=0\ . \tag{7}$$

The nontrivial solution of the above equation requires ψ to be expanded in terms of a complete set of functions ϕ_α's and expressing $G^0(E)$ and P in the same basis. This gives

$$D(E)=\left|\left|\delta_{\alpha\alpha'}-\sum_{\alpha''}G^0_{\alpha\alpha''}(E)P_{\alpha''\alpha'}\right|\right|=0\ , \tag{8}$$

where the elements of the Green's-function matrix are

$$G^0_{\alpha\alpha'}=\langle\alpha\,|\,E-H^0\,|\,\alpha'\rangle\ . \tag{9}$$

The condition of Eq. (8) determines the energy of the bound state while a general solution with energy E degenerates with the perfect crystal ($H^0\psi^0_{n\vec{k}}=E_{n\vec{k}}\psi^0_{n\vec{k}}$)is provided by the well-known Lippmann-Schwinger equation:

$$\psi=\psi^0+G^0(E)P\psi\ . \tag{10}$$

The solution of Eq. (10) allows examination of the effect of P upon the states in the valence and the conduction bands. To by pass the singularity at $E=E_{n\vec{k}}$, the definition of E and G^0 must be extended to include complex values. Thus,

$$G^0(E)\equiv\lim_{\epsilon\to0}(E-H^0+i\epsilon)^{-1}\ . \tag{11}$$

Rewriting Eq. (10) in the form

$$[I-G^0(E)P]\psi_{n\vec{k}}=\psi^0_{n\vec{k}}\ , \tag{12}$$

it can be noted that the determinant $D(E)$ $[\equiv||I-G^0(E)P||]$ is not vanishing as $G^0(E)$ is nonzero within the band continua. Thus, the solutions may exist at all energies within the energy bands of the crystal. Following Pantelides,[3] the phase shift $\gamma(E)$ (involving real and imaginary determinants) can be defined as

$$\gamma(E)=-\tan^{-1}\left[\frac{\mathrm{Im}D(E)}{\mathrm{Re}D(E)}\right]\ . \tag{13}$$

This suggests that whenever $\mathrm{Re}D(E)=0$ the quantity $\gamma(E)$ will be an odd multiple of $\pi/2$. An expansion around such an energy E_0 gives

$$\tan\gamma(E)=-\frac{\Gamma}{2(E-E_0)}\ , \tag{14}$$

with

$$\Gamma=\left[\frac{2\,\mathrm{Im}D(E)}{\mathrm{Re}\dfrac{d}{dE}D(E)}\right]_{E=E_0} \tag{15}$$

The solution for which $\Gamma>0$, one has a *resonance* or a peak in the change in density of states with half-width Γ. On the other hand, if $\Gamma<0$ the solution will provide an *antiresonance*, i.e., a negative peak in the change in density of states with half-width Γ.

III. NUMERICAL COMPUTATIONS AND RESULTS

A. Band structure and Green's functions

Following the method described in the Appendix, we have numerically evaluated the involved set of twenty-one tight-binding-interaction integrals to fit the existing pseudopotential data[31–33] for the perfect energy-band structures. Explicit calculations have been made for GaP, GaAs, GaSb, InP, InAs, InSb, and AlAs with the parameter values of Table I. The comparison of our band-structure calculation with the existing theoretical (nearest and next-nearest neighbor) and experimental data is given in Table II (see Figs. 1–7 also). It can be noted that our results provide fairly accurately the valence bands, band gaps, and relatively better conduction bands. In Figs. 8–14 we have displayed the calculated density of states that also agree well with the published theoretical and experimental x-ray photoelectron spectroscopy (XPS) data.

The matrix elements of the involved Green's functions can be evaluated numerically by incorporating the band structures (eigenvalues, $E_{n\vec{k}}$ and eigenvectors $|n\vec{k}\rangle$) of the host systems. Rewriting ing Eq. (9) in the generalized form

$$G^0_{\alpha\alpha'}(E)=\lim_{\epsilon\to0+}\sum_{n\vec{k}}\frac{\langle\alpha\,|\,n\vec{k}\rangle\langle n\vec{k}\,|\,\alpha'\rangle}{E-E_{n\vec{k}}+i\epsilon}\ , \tag{16}$$

and using the identity

$$\frac{1}{\chi-i\epsilon}=\mathcal{P}\frac{1}{\chi}-i\pi\delta(\chi)\ , \tag{17}$$

where $\mathcal{P}$ is the Cauchy principal value, one can write Eq. (16) in the form

$$G^0(E)=\mathcal{P}\int\frac{\delta(E'-H)}{E-E'}dE'-i\pi\delta(E-H^0)\ . \tag{18}$$

TABLE I. Tight-binding parameters (in eV) for III-V compounds of zinc-blende-type structure. The energy levels at critical points obtained from this set of parameters are compared with the pseudopotential data in Table II.

No. of interaction integrals[a]	GaP	GaAs	GaSb	AlAs	InP	InAs	InSb
$P_1=E_{ss}(000)0$	−6.284 78	−6.723 57	−6.092 77	−6.151 67	−6.294 08	−7.179 30	−6.839 22
$P_2=E_{ss}(000)1$	−2.789 20	−3.978 33	−3.885 60	−1.992 17	−3.428 65	−4.486 77	−3.914 58
$P_3=E_{xx}(000)0$	1.094 28	0.640 95	0.810 05	1.210 70	1.842 85	1.660 00	0.810 00
$P_4=E_{xx}(000)1$	2.382 00	2.874 07	2.347 75	2.331 75	2.608 85	2.335 62	2.662 10
$P_5=4E_{ss}(0.5,0.5,0.5)$	−7.750 00	−6.900 00	−6.350 00	−7.160 00	−6.300 00	−6.400 00	−5.800 00
$P_6=4E_{sx}(0.5,0.5,0.5)01$	5.260 00	5.240 00	5.100 00	5.252 00	4.800 00	5.400 00	4.570 00
$P_7=4E_{sx}(0.5,0.5,0.5)10$	4.870 00	4.321 00	4.110 00	4.050 00	4.080 00	4.000 00	3.850 00
$P_8=4E_{xx}(0.5,0.5,0.5)$	2.440 00	2.000 00	1.600 00	2.008 00	2.280 00	2.000 00	1.500 00
$P_9=4E_{xy}(0.5,0.5,0.5)$	5.560 00	5.500 00	5.500 00	4.850 00	5.300 00	5.460 00	5.290 00
$P_{10}=4E_{xx}(0,1,1)0$	−1.137 63	−0.339 05	−0.920 05	−1.120 60	−0.720 05	−0.824 10	−0.670 80
$P_{11}=4E_{xx}(0,1,1)1$	−1.186 10	−1.756 33	−2.012 15	−1.166 95	−1.338 15	−1.202 47	−2.007 10
$P_{12}=4E_{xy}(1,1,0)0$	0.760 00	0.600 00	0.760 00	0.760 00	0.520 00	0.550 00	0.600 00
$P_{13}=4E_{xy}(1,1,0)1$	1.330 00	0.960 00	1.330 00	1.330 00	0.910 00	0.880 00	0.960 00
$P_{14}=4E_{xx}(1,1,0)0$	0.854 47	0.444 45	0.599 40	0.552 20	0.384 15	0.227 35	0.472 20
$P_{15}=4E_{xx}(1,1,0)1$	1.189 20	1.120 77	1.007 80	1.105 35	0.739 10	0.983 13	0.710 70
$P_{16}=4E_{sx}(1,1,0)0$	0.024 00	0.045 20	0.042 00	0.040 00	0.087 00	0.056 00	0.081 00
$P_{17}=4E_{sx}(1,1,0)1$	0.083 20	0.096 40	0.060 00	0.073 00	0.102 00	0.086 00	0.094 00
$P_{18}=4E_{ss}(1,1,0)0$	−0.167 27	−0.047 38	−0.162 77	−0.025 57	−0.031 58	−0.092 40	−0.115 63
$P_{19}=4E_{ss}(1,1,0)1$	−0.181 40	−0.065 33	−0.224 40	−0.076 47	−0.034 15	−0.125 58	−0.119 77
$P_{20}=4E_{sx}(0,1,1)0$	1.180 00	0.780 00	0.750 00	0.540 00	0.900 00	0.840 00	0.780 00
$P_{21}=4E_{sx}(0,1,1)1$	−0.080 00	−0.080 00	−0.240 00	−0.120 00	−0.006 00	−0.080 00	−0.040 00
$P_{22}=4E_{xy}(0,1,1)0$	0	0	0	0	0	0	0
$P_{23}=4E_{xy}(0,1,1)1$	0	0	0	0	0	0	0

[a]In the notations of Slater and Koster, Ref. 22.

Again, the spectral density function, $\delta(E-H^0)$, in the above equation depends on the eigenvalues $E_{n\vec{k}}$ and eigenvectors $|n\vec{k}\rangle$,

$$\delta(E-H^0)=\sum_{n\vec{k}}|n\vec{k}\rangle\delta(E-E_{n\vec{k}})\langle n\vec{k}|\ , \tag{19}$$

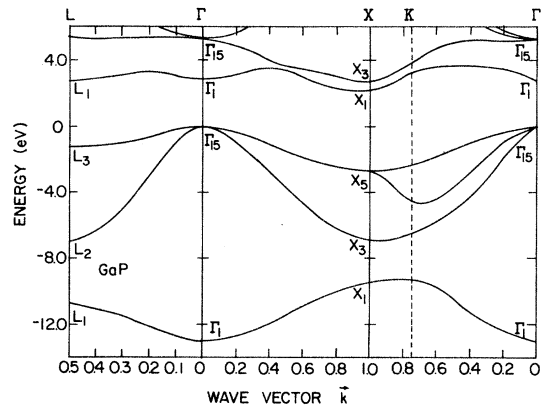

FIG. 1. Calculated band structure for GaP with the second-neighbor tight-binding parameters of Table I. For comparison with the energy values at critical points with the pseudopotential data of Chelikowsky and Cohen (Ref. 31) and other existing tight-binding calculations we have also included our results in Table II.

with the elements

$$\langle\alpha|\delta(E-H^0)|\alpha'\rangle=\sum_{n\vec{k}}\langle\alpha|n\vec{k}\rangle\times\delta(E-E_{n\vec{k}})\langle n\vec{k}|\alpha'\rangle\ . \tag{20}$$

Once the spectral density of states is obtained, the real and imaginary parts of the Green's functions $\langle\alpha|G^0(E)|\alpha'\rangle$ (with $\alpha=s$ or p) can be easily obtained by carrying out the principal-value in-

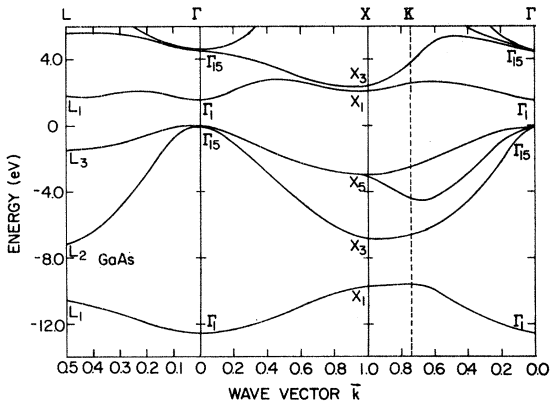

FIG. 2. Same key as Fig. 1, but for GaAs.

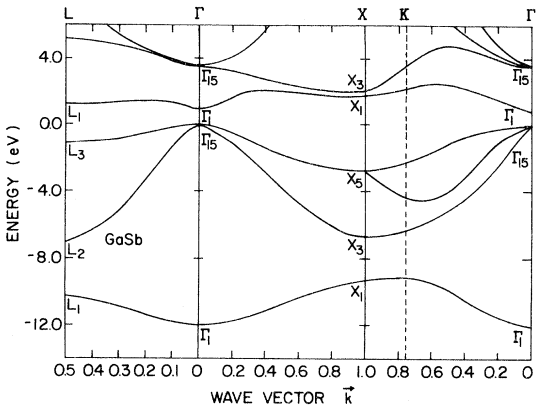

FIG. 3. Same key as Fig. 1, but for GaSb.

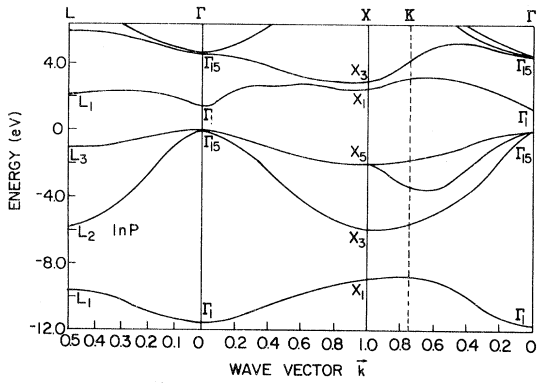

FIG. 4. Same key as Fig. 1, but for InP.

tegrals [Eq. (18)] using Simpson's rule.

The zeros of the diagonal matrix elements of the Green's functions [$\langle\alpha \mid G^0(E) \mid \alpha\rangle$, with $\alpha=s$ or p] within the band gap (if it exists) are identified as the bound states. The calculated results due to cation or anion vacancies in several III-V compounds are contained in Table III and compared with the existing theoretical and experimental data.

B. Neutral vacancy states in III-V compounds

For the last few years, the electronic states of point defects in III-V compounds have been extensively studied either by photoluminescence (PL), deep-level transient spectroscopy (DLTS), or by electron-paramagnetic-resonance (EPR) measure-

TABLE II. Energy levels of GaP, GaAs, and GaSb (in eV) at Γ, X, and L critical points. The results of our calculations obtained using parameters of Table I are compared with the existing theoretical and experimental data. The zero of the energy is considered at the top of the valence band.

		GaP				GaAs				
Critical point	Level	Calc.			Expt.	Calc.				Expt.
		Ref. 31	Ref. 27(b)	Ours	Ref. 52	Ref. 31	Ref. 28	Ref. 30[a]	Ours	Ref. 52
Γ	Γ_1^v	−12.99	−13.19	−13.00	−13.2±0.4	−12.55	−12.89	−11.99	−12.55	−12.9±0.5
	Γ_{15}^v	0.0	0.0	0.0		0.0	0.0	0.0	0.0	
	Γ_1^c	2.88	2.88	2.88		1.51	1.53	1.51	1.51	
	Γ_{15}^c	5.24	5.06	5.24		4.55	3.91	4.64	4.55	
X	X_1^v	−9.46	−9.694	−9.46	−9.6±0.3	−9.83	−9.96	−10.79	−9.83	−10.0±0.2
	X_3^v	−7.07	−6.89	−7.07	−6.9±0.3	−6.88	−6.08	−6.18	−6.88	−6.9±0.2
	X_5^v		−3.78	−2.70	−2.7±0.2	−2.99	−2.94	−2.48	−2.99	
	X_1^c	2.16	5.46	2.16		2.03	2.07	2.03	2.03	
	X_3^c	2.71	5.93	2.71		2.38	2.88	2.63	2.38	
L	L_1^v	−10.60	−10.91	−10.76		−10.60	−10.42	−10.75	−10.59	−12.0±0.5
	L_2^v	−6.84	−6.62	−7.03		−6.83	−7.19	−6.40	−7.20	
	L_3^v		−1.89	−1.32	−1.2±0.3	−1.42	−1.28	−1.23	−1.43	−1.4±0.3
	L_1^c	2.79	3.27	2.71		1.82	1.89	1.83	1.81	
	L_3^c		6.93	5.30		5.47	6.42	6.11	5.67	

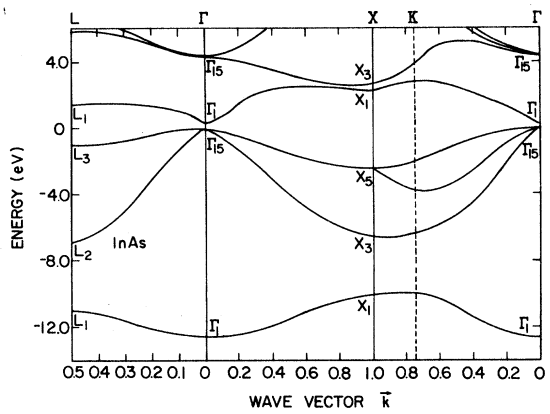

FIG. 5. Same key as Fig. 1, but for InAs.

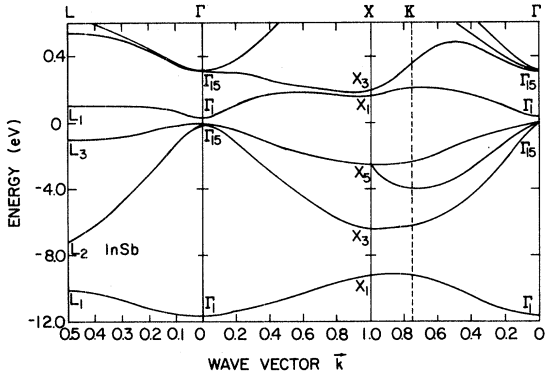

FIG. 6. Same key as Fig. 1, but for InSb.

ments.[1] Unfortunately, the identification of the defects and their respective properties have not been accurately predicted because of the inherent difficulties of using standard experimental techniques and also by the lack of reliable theoretical calculations. Very good progress in resolving the experimental uncertainties for detecting the EPR signals from defects has been made in recent years.[42–44] In GaP, the defects which have been identified by EPR method are P_{Ga} (antisite), V_{Ga} (vacancy at Ga), and an antisite impurity ($P_{Ga}-I$) pair. A PL study of native defects [V_P, V_{In}, P_i (interstitial), V_P-V_{In}, or V_P-P_i] in InP has also been made by Temkin *et al.*[44]

From theoretical stand point, an ideal vacancy with T_d symmetry (by simply removing either an anion or cation atom from an otherwise perfect lattice) in III-V compounds induces *twofold-* and *sixfold*-degenerate levels (including spin) with $a_1(s)$ and $t_2(p)$ symmetry, respectively. For the neutral anion (cation) vacancy there will be *three* (*five*) electrons associated with the bound levels. The a_1

TABLE II. (*Continued.*)

Critical point	Level	GaSb Calc. Ref. 31	GaSb Calc. Ref. 27(b)	GaSb Calc. Ref. 30[a]	GaSb Calc. Ours	GaSb Expt. Ref. 52	InP Calc. Ref. 31	InP Calc. Ref. 27(b)	InP Calc. Our	InP Expt. Ref. 52
Γ	Γ_1^v	−12.00	−11.61	−12.00	−12.00	−11.6±0.3	−11.42	−11.16	11.42	−11.0±0.4
	Γ_{15}^v	0.0	0.0	0.0	0.0		0.0	0.0	0.0	
	Γ_1^c	0.86	0.86	0.86	0.86		1.50	1.42	1.50	
	Γ_{15}^c	3.44	3.33	3.60	3.44		4.64	4.78	4.64	
X	X_1^v	−9.33	−9.40	−10.74	−9.33	−9.4±0.2	−8.91	−8.90	−8.91	−8.9±0.3
	X_3^v	−6.76	−6.91	−5.34	−6.76	−6.9±0.3	−6.01	−5.90	−6.01	−5.9±0.2
	X_5^v	−2.61	−3.44	−2.60	−2.61	−2.7±0.2	−2.09	−2.65	−2.09	−2.0±0.2
	X_1^c	1.72	3.66	1.72	1.72		2.44	4.95	2.44	
	X_3^c	1.79	5.19	1.79	1.79		2.97	5.04	2.97	
L	L_1^v	−10.17	−10.16	−10.77	−10.17		−9.67	−9.66	−9.79	
	L_2^v	−6.25	−6.51	−5.50	−6.25		−5.84	−5.47	−6.19	
	L_3^v	−1.45	−1.96	−1.34	−1.45	−1.3±0.2	−1.09	−1.35	−0.90	−1.0±0.3
	L_1^c	1.22	2.11	1.06	1.22		2.19	2.76	2.11	
	L_3^c	4.43	4.88	5.26	4.43		5.58	6.13	5.73	

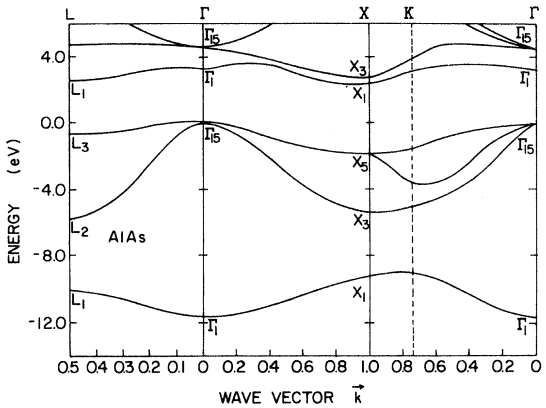

FIG. 7. Calculated band structure for AlAs with the second-neighbor tight-binding parameters of Table I. For comparison with the energy values at critical points with the pseudopotential data of Hess *et al.* (Ref. 32), Stukel *et al.* (Ref. 33), and the existing tight-binding calculations of Osbourn and Smith (Ref. 28 and quoted by Ref. 29), we have also included our results in Table II.

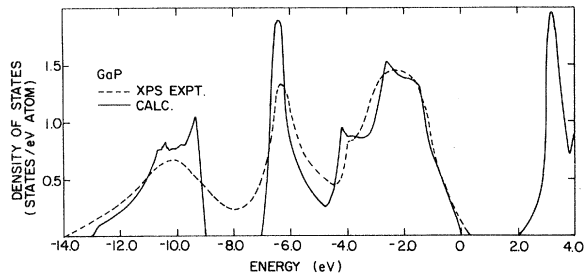

FIG. 8. Calculated electronic density of states for GaP with the second-neighbor tight-binding parameters of Table I compared with the XPS data of Ley *et al.*, Ref. 52.

(or *s*) state, occupied by two electrons, occurs at lower energy than the partially occupied [by *one* (*three*)] t_2 state.

In connection with the depth and the role of vacancy levels in elemental and compound semiconductors, various theoretical methods have provided different results.[11–21] Comparing the neutral vacancy levels in GaAs for example, our calculations for the bound state of t_2 symmetry for Ga vacancy agree reasonably well with those of Bernholc and Pantelides.[14] However, for the As vacancy we find only bound state of t_2 symmetry with energy 0.95 eV above the valence-band edge, where as the authors of Ref. 14 have obtained both levels of a_1 and t_2 type symmetries (with energies 0.71 and 1.47 eV). The most recent self-consistent calculations of Bachelet *et al.*[10] have provided justification to our semiempirical calculations. This also suggests that the results of Jaros and Brand[12] based on the pseudopotential framework and that of Faz-

TABLE II. (*Continued.*)

Critical point	Level	InAs Calc. Ref. 31	InAs Calc. Ref. 27(b)	InAs Calc. Ref. 30[a]	InAs Ours	InAs Expt. Ref. 52	InSb Calc. Ref. 31[b]	InSb Calc. Ref. 27(b)	InSb Calc. Ref. 30[a]	InSb Ours	InSb Expt. Ref. 52
Γ	Γ_1^v	−12.69	−12.30	−12.76	−12.69	−12.3±0.4	−11.71	−11.70	−12.26	−11.71	−11.7±0.3
	Γ_{15}^v	0.0	0.0	0.0	0.0		0.0	0.0	0.0	0.0	
	Γ_1^c	0.37	0.36	0.30	0.37		0.25	0.25	0.24	0.25	
	Γ_{15}^c	4.39	4.25	4.35	4.39		3.16	3.24	3.40	3.16	
X	X_1^v	−10.20	−10.20	−10.09	−10.20	−9.8±0.3	−9.20	−9.50	−9.56	−9.20	−9.0±0.3
	X_3^v	−6.64	−6.30	−6.89	−6.64	−6.3±0.2	−6.43	−6.41	−6.08	−6.43	−6.4±0.2
	X_5^v	−2.47	−2.82	−2.31	−2.47	−2.4±0.3	−2.45	−2.75	−2.05	−2.45	−2.4±0.4
	X_1^c	2.28	4.04	2.20	2.28		1.71	3.84	1.70	1.71	
	X_3^c	2.66	4.90	2.59	2.66		1.83	3.91	1.83	1.83	
L	L_1^v	−10.92	−10.88	−10.99	−10.99		−9.95	−10.23	−10.41	−10.03	
	L_2^v	−6.23	−5.86	−6.15	−6.87		−5.92	−5.94	−5.32	−6.81	
	L_3^v	−1.26	−1.57	−1.13	−1.05	−0.9±0.3	−1.44	−1.81	−1.03	−1.06	−1.05±0.3
	L_1^c	1.53	1.98	1.47	1.50		1.03	1.67	1.00	0.99	
	L_3^c	5.42	5.68	5.56	5.84		4.30	4.70	5.10	5.46	

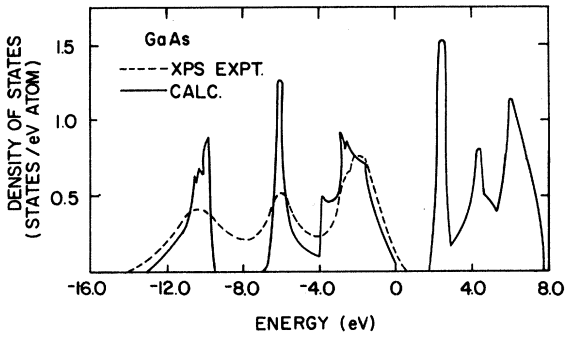

FIG. 9. Same key as Fig. 8 but for GaAs.

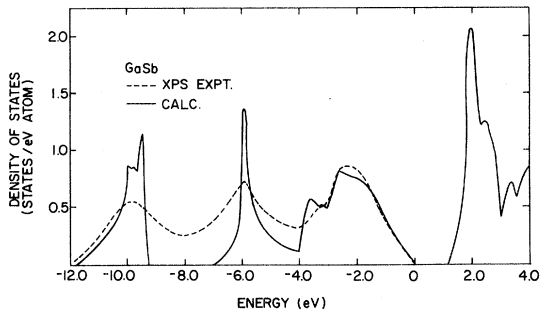

FIG. 10. Same key as Fig. 8 but for GaSb.

zio *et al.*[8] based on the cluster-model formalisms are at variance not only with ours, but with Bachelet *et al.*[10] as well. Following Pantelides,[3] we have displayed in Fig. 15 and Fig. 16 the results of our calculations for the changes in the density of states for Ga and As vacancy (in GaAs), respectively. Except for small discrepancies in the positions and structures, the overall agreement with the semiempirical and self-consistent[10] calculations is satisfactory.

Similar to GaAs and Si, our results for the neutral anion or cation vacancies in GaP, GaSb, and AlAs suggest that the states of a_1 symmetry are of *resonance* in character while the t_2 states will be of *localized* in nature (cf. Table III and Figs. 17 and 18). There are also differences exhibited in the pseudopotential results[12] for the anion vacancies in GaP and InP and the semiempirical calculations[16] for anion and cation vacancies in GaSb and InAs, respectively. Again, it is worth mentioning that except for a small difference (a few tenths of an eV) in the energy value for neutral Ga vacancy in GaP, our results are in corroboration with the most recent self-consistent pseudopotential calcula-

TABLE II. (*Continued.*)

Critical point	Level	AlAs Calc. Ref. 33	Ref. 32	Ref. 28	Our
Γ	Γ_1^v	−11.48	−11.66	−12.06	−11.66
	Γ_{15}^v	0.0	0.0	0.0	0.0
	Γ_1^c	2.50	3.21	2.82	3.21
	Γ_{15}^c	4.57	4.57	4.19	4.57
X	X_1^v	−9.61	−9.42	−9.46	−9.42
	X_3^v	−5.20	−5.55	−5.02	−5.54
	X_5^v	−2.01	−1.97	−1.72	−1.97
	X_1^c	2.38	2.25	2.30	2.25
	X_3^c	2.86	2.62	3.01	2.61
L	L_1^v	−10.14	−10.07	−9.94	−10.21
	L_2^v	−5.22	−5.52	−5.85	−5.87
	L_3^v	−0.80	−0.70	−0.48	−0.71
	L_1^c	2.57	2.76	2.64	2.73
	L_3^c	5.25	5.15	4.81	4.58

[a]We have set the positions of the energy levels considering zero as the top of the valence band in the calculations of Ref. 30 to compare it with our results.

[b]There are some discrepancies in the quoted and plotted energy levels for InSb.

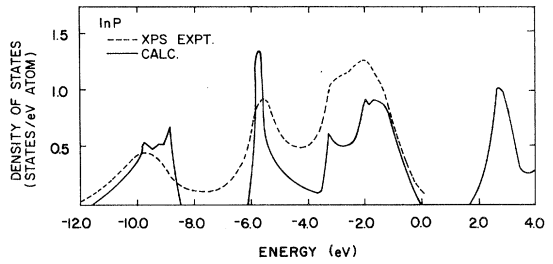

FIG. 11. Same key as Fig. 8 but for InP.

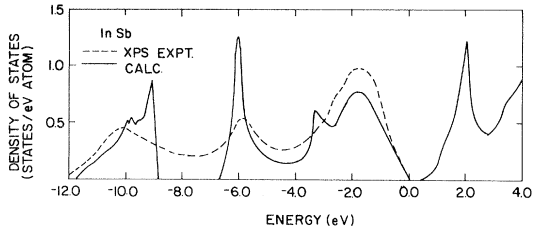

FIG. 13. Same key as Fig. 8 but for InSb.

tion of Scheffler *et al.*[21]

In Fig. 19 we have displayed results for the calculated position of the highest occupied levels for anion and cation vacancies in III-V compounds as a function of the ionicity scale of Phillips.[46] With respect to the valence-band maximum (considered at zero energy), the positions of these levels are found to decrease approximately with the increase of the covalency (or decrease of the ionicity). Again, one can note that for Ga-In pnictides (i.e., GaAs-InAs, GaP-InP, and GaSb-InSb) the pinning energies of the anion vacancy levels of t_2 symmetry are almost the same while they are different for Ga-Al and In-Al compounds (i.e., GaAs-AlAs and InAs-AlAs, see Table III). On the other hand, we find no such correlation of pinning energies with the cation vacancy levels.

In III-V compounds, it has been speculated that impurities near the surface are responsible for determining the position of the Fermi level (E_F) relative to the surface band edge.[47–51] Although the defects that pin E_F are not well understood, but there is ample experimental evidence which suggests that simple vacancies are first formed that later interact with the other lattice atoms to form complexes (for an excellent survey of the experimental data see Spicer *et al.*[47]). Quite recently, Daw and Smith[37] have reported calculations for the bound-state energy levels of ideal vacancies near the (110) surface of InP and GaAlAs. These authors have found a strong correlation between the calculated position of the highest-filled, ideal anion vacancy level with the surface Fermi level while no connection with the measured Fermi level and the highest-occupied cation vacancy level has been noticed. Another recent experimental observation that might be significant in correlating the role of the anion vacancies in Fermi-level pinning is that of Keuch and McCaldin[36] in which the variation of E_F as a function of the alloy composition in mixed compounds has been reported. For $In_xGa_{1-x}As(P)$ systems the variation of the Fermi level is found to be independent of x while it increases linearly with aluminum content in $Ga_{1-x}Al_xAs$ (Ref. 51) ternary. Since the same trend is exhibited for the highest-occupied level in the neutral anion vacancy in the bulk and on the (110) surface in III-V compounds, we therefore believe that our results for the anion vacancy levels for GaP-InP, GaAs-InAs, and GaAs-AlAs are in corroboration with the existing experimental trends. This provides justification at least to some extent that the anion vacancies near the surface are responsible for determining the position of the Fermi level and also lends support to the speculation of Keuch and McCaldin that similar to GaInAs(P)

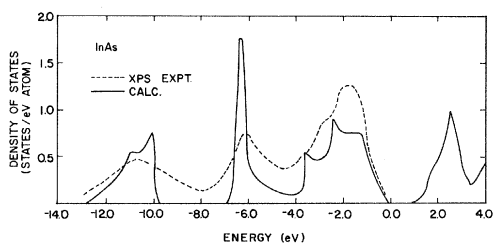

FIG. 12. Same key as Fig. 8 but for InAs.

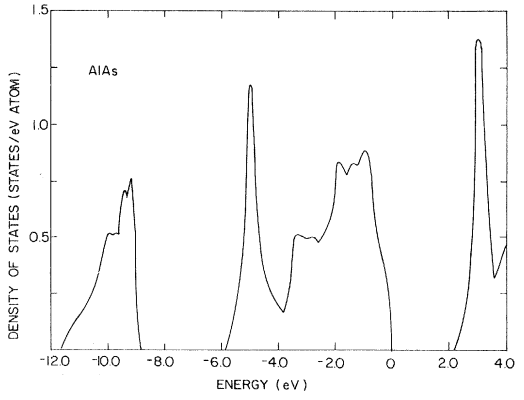

FIG. 14. Calculated electronic density of states for AlAs with the second-neighbor tight-binding parameters of Table I.

TABLE III. The positions of the energy levels found within the band gap of a_1 and t_2 symmetries due to neutral vacancies in III-V compounds. The values of the calculated energy gap for the host systems E_g are also reported. All the energies are measured in eV considering zero as the top of the valence-band edge.

System	Ours			Others		
	E_g	a_1	t_2	a_1	t_2	Reference
*Al*As:V	2.25		0.54			
Al*As*:V			1.60			
*Ga*P:V	2.15		0.24	0.35	0.15	b
Ga*P*:V			1.54			b
*Ga*As:V	1.5		0.05		0.03(0.55)(~0.06)	c,d,e
Ga*As*:V			0.95	0.71(0.86)	1.47(1.33)(resonance)(1.08)	c,d,e,f
*Ga*Sb:V	0.86		0.08		~0.47	i
Ga*Sb*:V			0.61	0.71	0.80~(0.42)	g,i
*In*P:V	1.50		0.54			b
In*P*:V		0.28	1.50	0.12		g
*In*As:V	0.37		0.38[a]	0.20	0.25	
In*As*:V		0.19	0.92[a]			
*In*Sb:V	0.25		0.05			
In*Sb*:V			0.59[a]			

[a]Resonance levels lying within the conduction bands.
[b]Reference 12.
[c]Reference 14.
[d]Reference 8.
[e]Reference 12(c).
[f]Reference 10.
[g]Reference 16.
[h]Reference 21.
[i]Reference 8(b). (L. M. Brescamsin *et al.*)

ternaries, the Fermi-level variation for GaSb-InSb systems should be independent of the composition factor.

C. Deep traps associated with short-range potentials in III-V compounds

In order to have an adequate representation of the effective impurity potential for defining the defect to be a deep trap in a given host system, it requires precise considerations of the effects like Coulomb interactions,[1-4] lattice relaxation, and charge-state splitting, etc. Unfortunately, any unified theory where all the effects can be included to predict the deep impurity level with accuracy does not exist. However, for the isoelectronic impurities (without Coulomb interactions) and neglecting the effects of lattice relaxation, the Green's-function method in the molecular picture might be the simplest one at least to understand qualitatively and to predict how a given impurity level will change with the alteration of the host atom. Similar to Hjalmarson *et al.*,[15] if we restrict ourself to the case where the impurity potential is confined to the central cell alone, then the perturbation matrix will depend on the change in the on-site energies as well as on the change in the transfer matrix elements. Since the transfer matrix elements depend approximately on the bond length, for the case when the impurity and the host lattice atoms are of the same size (or no relaxation), it is plausible to consider the change in the transfer matrix elements

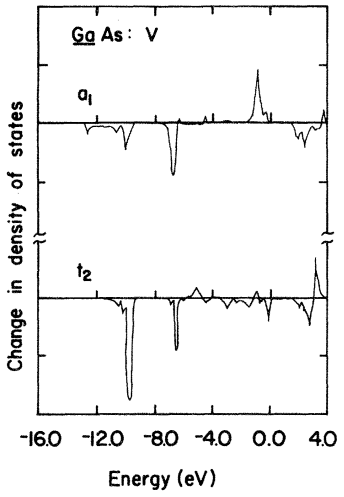

FIG. 15. The contributions of a_1 and t_2 symmetries to the change in the density of states caused by an isolated Ga vacancy in *Ga*As:V. Calculations are made on the lines of the method given in Ref. 14.

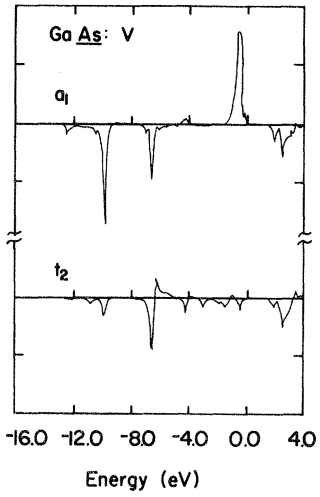

FIG. 16. Same key as Fig. 15, but for Ga*As*:V.

(which will be negligible small) to be zero. In this respect the perturbation matrix will be diagonal and the calculated Green's functions can be used to predict the deep-trap energies associated with the impurities occupying either anion or cation sites, respectively.

In Figs. 20 and 21 we have displayed the results of our calculations for III-V compounds that predict the occurrence of deep traps of a_1 and t_2 symmetry due to the short-range impurity potential

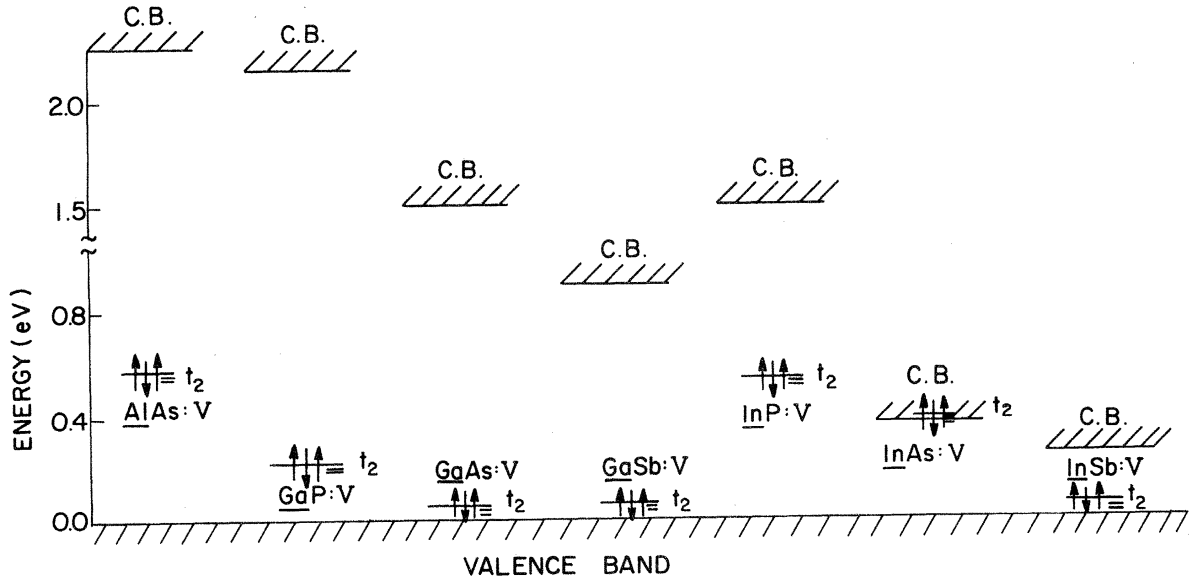

FIG. 17. Calculated positions of the localized states due to cation vacancies in the III-V compounds. The zero of the energy is considered at the top of the valence band where CB represents the lower part of the conduction band (see Table III also).

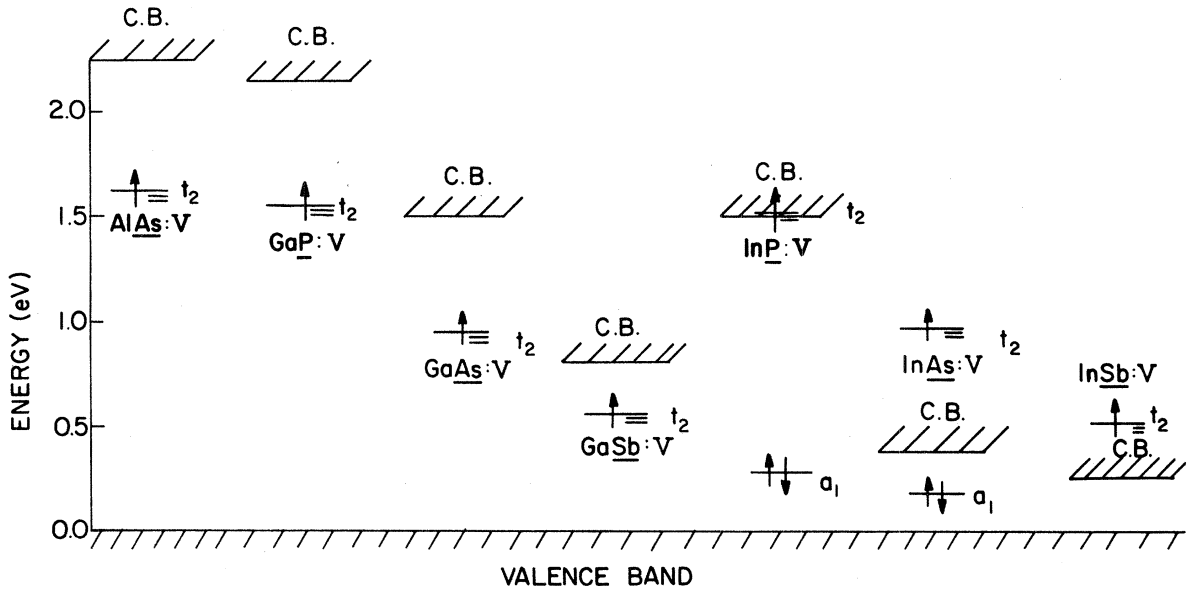

FIG. 18. Same key as Fig. 17 but for anion vacancies in the III-V compounds.

at the cation site. An a_1-type state, which is pulled out of the conduction band can be a localized one if the impurity potential is attractive and also if it is greater than a critical value. On the other hand, one can obtain bound states of t_2 symmetry, both for the attractive as well as for the repulsive potentials. Again, one can note from Fig. 21 that as the impurity potential tends to $\pm$infinity, the energy of the deep traps becomes pinned to the energy equal to the t_2 bound state of an ideal cation vacancy (as given in Table III). Similar behavior will exhibit for the a_1 and t_2 states

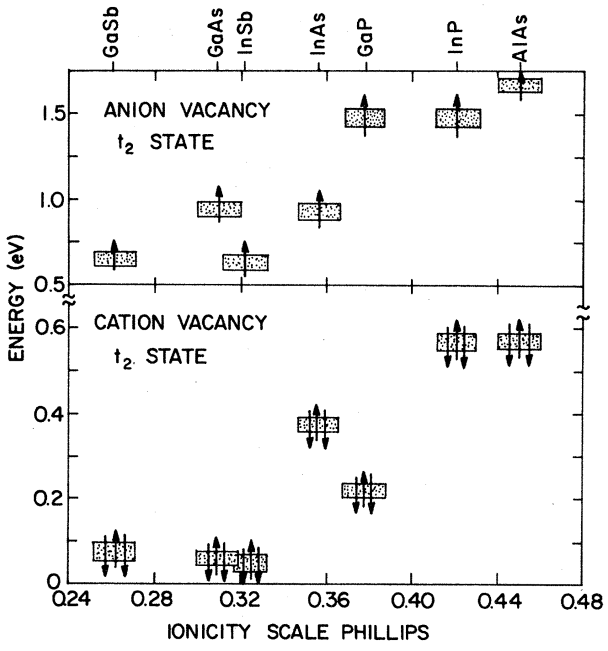

FIG. 19. Variation of the highly occupied t_2 states of anion and cation vacancies in III-V compounds vs ionicity scale of Phillips.

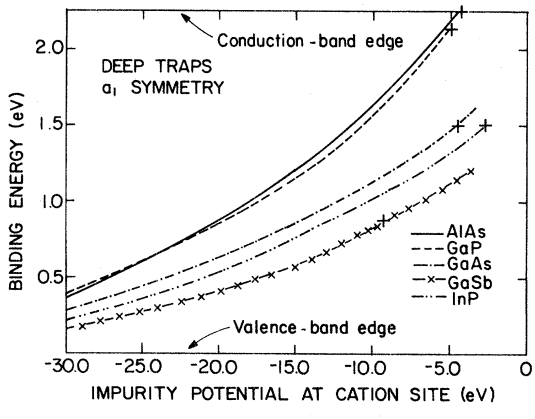

FIG. 20. Predicted energies of the deep traps of a_1 symmetry in III-V compound semiconductors with respect to the central-cell impurity potential at the cation site. The zero of the energy is considered at the top of the valence band, whereas (+) signs designate the lower part of the conduction band in each of the compounds considered here.

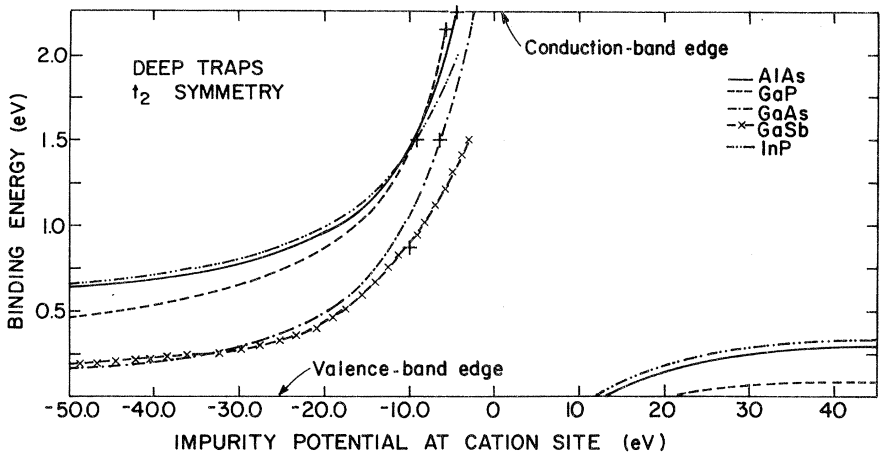

FIG. 21. Same key as Fig. 20 but for the deep traps of t_2 symmetry.

due to a short-range impurity potential at the anion site. Unfortunately, there is not sufficient experimental data for isoelectronic traps to be compared with the present theoretical results, however, we have noticed an increasing interest of antisite defects in GaP and GaAs systems that can be useful for approximately checking the reliability of our calculations.

Quite recently, Wagner *et al.*[43] have observed an electron-spin-resonance (ESR) signal from a partially filled symmetric state in GaAs which they have attributed to an As antisite defect. Similar experimental speculation for P antisite defect in GaP has already been reported by Kaufman *et al.*[41]. Assuming the potential due to an As impurity occupying the Ga site as the difference in their respective atomic energies, one can approximately calculate the possible occurrence of the antisite defect levels in GaAs and other III-V compounds to check the qualitative significance of the calculations. We have found a symmetric a_1 bound state close to the edge of the conduction band ($E_v+1.4$ eV) in GaAs while for P antisite defect in GaP the symmetric bound level occurs at energy ($E_v+2.0$ eV), respectively. On the other hand, the graphical solution of t_2 symmetry for the antisite As and P defects in GaAs and GaP will provide two *hyperdeep* resonance levels, one each in the valence and the conduction bands, respectively. Our results which provide support to the experimental observations differ in energy by few tenths of an eV from a recent theoretical semiempirical calculations by Lin-Chung and Reinecke.[38] However the basic trends for the a_1 and t_2 symmetry levels are found to be very much similar. Again, support to our results for an antisite P_{Ga} defect in GaP from the most recent self-consistent calculation of Scheffler *et al.*,[21] is also worth mentioning. Furthermore, except for the narrow gap semiconductors (e.g., GaSb, InAs, and InSb) we predict the possibility of the symmetric bound levels of antisite P and As defects in InP and AlAs respectively, to be detected by the future experiments.

IV. CONCLUSIONS

The electronic properties of neutral vacancies and substitutional impurities in III-V compounds have been studied in the Green's-function framework and using the tight-binding method. A total of *eight* tight-binding wave functions per unit cell were used in the band structure, giving an (8×8) matrix to be diagonalized for the energy eigenvalues and eigenvectors. The eight wave functions produced four valence bands and four conduction bands. All possible interactions up to and including second neighbors have been considered. Using symmetric arguments, the number of such parameters in zinc-blende-type crystals are reduced to twenty-three. In view of the existing pseudopotential data,[31–33] we are able to calculate the twenty-one interaction integrals in a systematic way using least-square-fitting technique (cf. Appendix). When compared with the existing tight-binding calculations, our set of parameters provide much better fit to the pseudopotential[31–33] and/or the ex- we have calculated the Green's functions (by generating the eigenvalues and eigenfunctions throughout the Brillouin zone) and there by the perimental[52] (wherever known) energy levels. Having determined the reliable set of bulk parameters,

isolated anion-cation vacancy levels in III-V compounds. The calculated results have been compared and discussed with the existing theoretical data.

Similar to GaAs and Si, our results for the ideal cation and anion vacancies in GaP, GaSb, and AlAs suggest that the states of a_1 symmetry are of resonance in character while the t_2 states will be of localized in nature (cf. Table III and Figs. 17 and 18). However, the situation for the anion vacancies in InP and InAs is found to be different (cf. Fig. 18). It has been noticed that there exists a deep-bound level of a_1 symmetry within the band gap and their respective energies decrease approximately with the decrease of the ionicity. On the basis of the calculated deep-level energies we find that the anion vacancies are more important defects rather than the cation vacancies. While comparing the calculated energy levels with experiments, it is to be mentioned that the lattice surrounding a vacancy will undergo Jahn-Teller distortions which have been completely neglected here. The relaxation of the atoms surrounding the vacancy will lower the energy of the ideal vacancy by few tenths of an eV and it is expected that the anion vacancy levels, would still be highly deep. The overall trends between theory and the existing experimental data for the anion vacancies are generally very encouraging.

For cation vacancies on the other hand, it has been pointed out by Watkins[53] that metal vacancy in II-VI compounds exhibits large Jahn-Teller distortions. Although, the possibility of an E_3 level as being due to the isolated Ga vacancy in GaAs was suggested by Lang *et al.*,[54] but this speculation has been ruled out quite recently by Wallis *et al.*,[55] on the basis of their detailed pressure-dependent DLTS measurements. Again, the method by which Kennedy and Wilsey[43] attributed the EPR signal to be the V_{Ga} in electron-irradiated GaP, has also been questioned by Scheffler *et al.*[21] on the basis of their self-consistent pseudopotential calculations. Our semiempirical results are in corroboration with the findings of Ref. 21 (see Table III). Since any partial occupation of the degenerate triplet (t_2) level will be unstable to a distortion to a lower symmetry, only the detailed calculations[19] of the charge states of the relaxed cation vacancies would provide a reasonable comparison to the experimental results. Again, as the position of the partially occupied t_2 cation vacancy states in III-V compounds varies approximately with the increase of the ionicity (see Fig. 19) one can therefore speculate that the cation vacancy states in II-VI compounds will be highly deep[13] and may exhibit large Jahn-Teller distortions (in concurrence with the findings of Watkins[56]).

The occurrence of antisite defect levels [viz., $As(P)_{Ga}$ in GaAs(P)] has been also calculated approximately by assuming the potential due to As(P) occupying a Ga site is the difference in their respective atomic energies. Without accounting for the relaxation and confining the impurity potential to the central cell alone, it is plausible to assume the small changes in the transfer matrix elements in the perturbation to be zero. In this simplified picture the calculated results for the *antisite* defect levels in GaAs and GaP are found to be consistent with the existing theoretical[51] and experimental data.[42–44] Although, in the empirical tight-binding calculations there might be some uncertainties in the absolute values of the calculated impurity levels, the basic trends in light of the recent sophisticated self-consistent calculations are quite analogous. Finally, the simplicity in the computational work has provided the tight-binding method a potential to treat qualitively not only the isolated impurities (vacancies) in semiconductors, but also in principle, the incentive to extend it for the electronic structure of more complex defects[26] (e.g., divacancies, surfaces, and interfaces, etc.). These problems are under consideration and the results will be reported elsewhere.

Note added. We find analogous calculations for the isolated vacancies in III-V compounds reported recently by S. Das Sarma and A. Madhukar [Phys. Rev. B 24, 2651 (1981)]. However, the results of deep levels are seen to be substantially different not only with ours but with their own previous data (Ref. 16) as well as the most recent self-consistent calculations (Ref. 10 and Ref. 21). The discrepancies in the calculations are likely to be due to their arbitrary choice of tight-binding parameters for describing the band structure. Our set of parameters which have been obtained by the nonlinear least-squares-fit method (see Table I and the Appendix) are significantly different from theirs.

ACKNOWLEDGMENTS

We are benefited by the valuable discussions on the subject matter with M. Schlüter, R. E. Allen, P. J. Lin-Chung, and T. L. Reinecke. This work has been supported in part by an ONR Contract No. NO0014-78-CO508.

APPENDIX

In the notations of Slater and Koster, and following Dresselhaus and Dresselhaus,[39] the elements of the (8×8) secular determinant representing all possible interactions up to and including second neighbors in the tight-binding framework with sp^3 orbitals centered on each atom for the perfect zinc-blende-type crystals, are given by

$$
\begin{aligned}
&\langle s_0 \mid s_0\rangle = E_{ss}(000)_0 + 4E_{ss}(110)_0(C_1C_2 + C_2C_3 + C_3C_1) ,\\
&\langle s_0 \mid s_1\rangle = 4E_{ss}(0.5,0.5,0.5)g_0 ,\\
&\langle s_1 \mid s_1\rangle = E_{ss}(000)_1 + 4E_{ss}(110)_1(C_1C_2 + C_2C_3 + C_3C_1) ,\\
&\langle s_0 \mid p_{x0}\rangle = -4E_{sx}(011)_0S_2S_3 + 4iE_{sx}(110)_0S_1(C_2 + C_3) ,\\
&\langle s_1 \mid p_{x0}\rangle = -4E_{sx}(0.5,0.5,0.5)_{10}g_1^* ,\\
&\langle p_{x0} \mid p_{x0}\rangle = E_{xx}(000)_0 + 4E_{xx}(110)_0C_1(C_2 + C_3) + 4E_{xx}(011)_0C_2C_3 ,\\
&\langle s_0 \mid p_{y0}\rangle = -4E_{sx}(011)_0S_1S_3 + 4iE_{sx}(110)_0S_2(C_3 + C_1) ,\\
&\langle s_1 \mid p_{y0}\rangle = -4E_{sx}(0.5,0.5,0.5)_{10}g_2^* ,\\
&\langle p_{x0} \mid p_{y0}\rangle = -4E_{xy}(110)_0S_1S_2 - 4iE_{xy}(011)_0C_3(S_1 - S_2) ,\\
&\langle p_{y0} \mid p_{y0}\rangle = E_{xx}(000)_0 + 4E_{xx}(110)_0C_2(C_1 + C_3) + 4E_{xx}(011)_0C_1C_3 ,\\
&\langle s_0 \mid p_{z0}\rangle = -4E_{sx}(011)_0S_1S_3 + 4iE_{sx}(110)_0S_3(C_1 + C_2) ,\\
&\langle s_1 \mid p_{z0}\rangle = -4E_{sx}(0.5,0.5,0.5)_{10}g_3 ,\\
&\langle p_{x0} \mid p_{z0}\rangle = -4E_{xy}(110)_0S_1S_3 - 4iE_{xy}(011)_0C_2(S_1 - S_3) ,\\
&\langle p_{y0} \mid p_{z0}\rangle = -4E_{xy}(110)_0S_2S_3 - 4iE_{xy}(011)_0C_1(S_2 - S_3) ,\\
&\langle p_{z0} \mid p_{x0}\rangle = E_{xx}(000)_0 + 4E_{xx}(110)_0C_3(C_1 + C_2) + 4E_{xx}(011)_0C_1C_2 ,\\
&\langle s_0 \mid p_{x1}\rangle = 4E_{sx}(0.5,0.5,0.5)_{01}g_1 ,\\
&\langle s_1 \mid p_{x1}\rangle = 4E_{sx}(011)_1S_1S_2 + 4iE_{sx}(110)S_1(C_2 + C_3) ,\\
&\langle p_{x0} \mid p_{x1}\rangle = 4E_{xx}(0.5,0.5,0.5)g_0 ,\\
&\langle p_{y0} \mid p_{x1}\rangle = 4E_{xy}(0.5,0.5,0.5)g_3 ,\\
&\langle p_{z0} \mid p_{x1}\rangle = 4E_{xy}(0.5,0.5,0.5)g_2 ,\\
&\langle p_{x1} \mid p_{x1}\rangle = E_{xx}(000)_1 + 4E_{xx}(110)_1C_1(C_2 + C_3) + 4E_{xx}(011)_1C_2C_3 ,\\
&\langle s_0 \mid p_{y1}\rangle = 4E_{sx}(0.5,0.5,0.5)_{01}g_2 ,\\
&\langle s_1 \mid p_{y1}\rangle = 4E_{sx}(011)_1S_1S_3 + 4iE_{sx}(110)_1S_2(C_1 + C_3) ,\\
&\langle p_{x0} \mid p_{y1}\rangle = 4E_{xy}(0.5,0.5,0.5)g_3 ,\\
&\langle p_{y0} \mid p_{y1}\rangle = 4E_{xx}(0.5,0.5,0.5)g_0 ,\\
&\langle p_{z0} \mid p_{y1}\rangle = 4E_{xy}(0.5,0.5,0.5)g_1 ,\\
&\langle p_{x1} \mid p_{y1}\rangle = -4E_{xy}(110)_1S_1S_2 + 4iE_{xy}(011)_1C_3(S_1 - S_2) ,\\
&\langle p_{y1} \mid p_{y1}\rangle = E_{xx}(000)_1 + 4E_{xx}(110)_1C_2(C_3 + C_1) + 4E_{xx}(011)_1C_1C_3 ,\\
&\langle s_0 \mid p_{z1}\rangle = 4E_{sx}(0.5,0.5,0.5)_{01}g_3 ,\\
&\langle s_1 \mid p_{z1}\rangle = 4E_{xy}(011)_1S_1S_2 + 4iE_{sx}(110)_1S_3(C_1 + C_2) ,
\end{aligned}
\tag{A1}
$$

$$\langle p_{x0}|p_{z1}\rangle = 4E_{xy}(0.5,0.5,0.5)g_2 ,$$

$$\langle p_{y0}|p_{z1}\rangle = 4E_{xy}(0.5,0.5,0.5)g_1 ,$$

$$\langle p_{z0}|p_{z1}\rangle = 4E_{xx}(0.5,0.5,0.5)g_0 ,$$

$$\langle p_{x1}|p_{z1}\rangle = -4E_{xy}(110)_1 S_1 S_3 + 4iE_{xy}(011)_1 C_2 (S_1 - S_3) ,$$

$$\langle p_{y1}|p_{z1}\rangle = -4E_{xy}(110)_1 S_2 S_3 + 4iE_{xy}(011)_1 C_1 (S_2 - S_3) ,$$

$$\langle p_{z1}|p_{z1}\rangle = E_{xx}(000)_1 + 4E_{xx}(110)_1 C_3 (C_1 + C_2) + 4E_{xx}(011) C_1 C_2 .$$

$$\ldots$$

with

$$C_1 = \cos\pi k_x , \quad S_1 = \sin\pi k_x ,$$

$$C_2 = \cos\pi k_y , \quad S_2 = \sin\pi k_y ,$$

$$C_3 = \cos\pi k_z , \quad S_3 = \sin\pi k_z ,$$

and

$$g_0 = \cos(\pi k_x/2)\cos(\pi k_{y/2})\cos(\pi k_z/2) - i\sin(\pi k_x/2)\sin(\pi k_y/2)\sin(\pi k_z/2) ,$$

$$g_1 = -\cos(\pi k_x/2)\sin(\pi k_y/2)\sin(\pi k_z/2) + i\sin(\pi k_x/2)\cos(\pi k_y/2)\cos(\pi k_z/2) ,$$

$$g_2 = -\sin(\pi k_x/2)\cos(\pi k_y/2)\sin(\pi k_z/2) + i\cos(\pi k_x/2)\sin(\pi k_y/2)\cos(\pi k_z/2) ,$$

$$g_3 = -\sin(\pi k_x/2)\sin(\pi k_y/2)\cos(\pi k_z/2) + i\cos(\pi k_x/2)\cos(\pi k_y/2)\sin(\pi k_z/2) .$$

The terms $g_0^*, g_1^*, \ldots$ are the complex conjugates of $g_0, g_1, \ldots$ and $E_{ss}(000)_0, E_{ss}(000)_1, \ldots$ are the twenty-three interaction integrals ($P_1 - P_{23}$ given in Table I). The atomic orbitals s_0, p_{x0}, p_{y0}, and p_{z0} are assumed to be centered on the anion while s_1, p_{x1}, p_{y1}, and p_{z1} are supposed to be centered on the cation in our notations.

Calculations of the interaction integrals. In order to understand the transport properties of the perfect-diamond-type crystals, Dresselhaus *et al.*[39] and Bortolani *et al.*[56] have adjusted the involved parameters in such a way so as to reproduce the effective masses and the optical transitions. However, a comparison with the photoemission experiments or with the direct calculations of the band structure shows large discrepancies in their energy values (see Pandey and Phillips[24] for detailed comparison). By incorporating the eigenvalues at critical points as an input, Pandey and Phillips[24] were successful in providing the correct shape of the valence bands and relatively better results than those of Chadi and Cohen.[27] However, with their simplified tight-binding scheme, the conduction bands are not adequately represented and moreover the values for the band gap are generally overestimated.

With interaction integrals up to and including second neighbors, the electronic properties of the super lattices [e.g., AlAs-GaAs (001) and InAs-GaSb (001)] have been reported recently in the tight-binding approximation. Schulman and McGill[29] have incorporated the band-structure parameterization of Osbourn and Smith[28], while Nucho and Madhukar[30] have reported their own sets of parameters for InAs, GaAs, InSb, and GaSb. The magnitudes of our parameter values and their signs are consistent with those reported in Ref. 28, however, we have achieved a relatively better fit for GaAs and AlAs than those of Osbourn and Smith (cf. Table II). Unlike Nucho and Madhukar,[30] we feel that the choice of the top of upper valence band as a reference level (at zero energy) for all the elemental and compound semiconductors can provide us at least a consistent set of tightbinding parameters which otherwise can not be achieved. The results of their calculations have also been included in Table II for comparisons and contrasts with our calculations.

We have numerically evaluated the involved set of (twenty-one) interaction integrals by incorporat-

ing the pseudopotential data of energy bands at critical points as an input and using nonlinear least-squares-fit method. The dependence of the energies on the involved parameters can be obtained in a closed form along high-symmetry directions and at some critical points. Using Eqs. (A1) the energy eigenvalues at the Γ critical point are given by

$$\left.\begin{aligned} E(\Gamma_{1c}) &= \left[\frac{A+B}{2}\right] + \left[\left[\frac{A-B}{2}\right]^2 + P_5^2\right]^{1/2}, \\ E(\Gamma_{1v}) &= \left[\frac{A+B}{2}\right] - \left[\left[\frac{A-B}{2}\right]^2 + P_5^2\right]^{1/2}, \\ E(\Gamma_{15c}) &= \left[\frac{C+D}{2}\right] + \left[\left[\frac{C+D}{2}\right]^2 + P_8^2\right]^{1/2} \\ E(\Gamma_{15v}) &= \left[\frac{C+D}{2}\right] - \left[\left[\frac{C+D}{2}\right]^2 + P_8^2\right]^{1/2} \end{aligned}\right\} \text{ triply degenerate .} \tag{A2}$$

Similarly at X critical point (with $k_x=1$, $k_y=k_z=0$) we may get

$$\left.\begin{aligned} E(X_{3c}) &= \left[\frac{E+F}{2}\right] + \left[\left[\frac{E-F}{2}\right]^2 + P_7^2\right]^{1/2}, \\ E(X_{3v}) &= \left[\frac{E+F}{2}\right] - \left[\left[\frac{E-F}{2}\right]^2 + P_7^2\right]^{1/2}, \\ E(X_{1c}) &= \left[\frac{G+H}{2}\right] + \left[\left[\frac{G-H}{2}\right]^2 + P_6^2\right]^{1/2}, \\ E(X_{1v}) &= \left[\frac{G+H}{2}\right] - \left[\left[\frac{G-H}{2}\right]^2 + P_6^2\right]^{1/2}, \\ E(X_{5c}) &= \left[\frac{I+J}{2}\right] + \left[\left[\frac{I-J}{2}\right]^2 + P_9^2\right]^{1/2} \\ E(X_{5v}) &= \left[\frac{I+J}{2}\right] - \left[\left[\frac{I-J}{2}\right]^2 + P_9^2\right]^{1/2} \end{aligned}\right\} \text{ doubly degenerate .} \tag{A3}$$

The doubly degenerate energy values at the L critical point are given by

$$\left.\begin{aligned} E(L_{3c}) &= \left[\frac{K+L}{2}\right] + \left[\left[\frac{K-L}{2}\right]^2 + \left[\frac{(P_8+P_9)}{2}\right]^2\right]^{1/2}, \\ E(L_{3v}) &= \left[\frac{K+L}{2}\right] - \left[\left[\frac{K-L}{2}\right]^2 \left[\frac{P_8+P_9}{2}\right]^2\right]^{1/2}, \end{aligned}\right. \tag{A4}$$

where

$$A = P_1 + 3P_{18} ,$$

$$B = P_2 + 3P_{19} ,$$

$$C = P_3 + 2P_{14} + P_{10} ,$$

$$D = P_4 + 2P_{15} + P_{11} ,$$

$$E = P_2 - P_{19} ,$$

$$F = P_3 - 2P_{14} + P_{10} ,$$

and

$$G = P_1 - P_{18} ,$$

$$H = P_4 - 2P_{15} + P_{11} ,$$

$$I = P_3 - P_{10} ,$$

$$J = P_4 - P_{11} ,$$

$$K = P_3 + P_{12} ,$$

$$L = P_4 + P_{13} .$$

The above equations (A2), (A3), and (A4) will be reduced to those reported by Chadi and Cohen[27] if only nearest neighbor interactions are considered. Using Eqs. (A2), (A3), and (A4), with the involved parameters, one can reproduce fairly accurately the energy eigenvalues at Γ, X, and L (L_{3c} and L_{3v} doubly degenerate only) critical points. The nondegenerate energy values at L point (e.g., L_{1v}, L_{1c}, L_{2v}, etc.) can further be improved by a suitable choice of P_{20} and P_{21}, respectively. On the other hand, P_{16} and P_{17}, can be used to achieve a better fit in the energy values at K critical point. As the pseudopotential data is known for high-symmetry directions only, we have therefore neglected P_{22} and P_{23} which are dependent on the energy values along $(k_x, k_{y/2}, 0)$.

The resulting bulk band structures with the values of our parameters of Table I are shown in Figs. 1—6. Comparing the existing pseudopotential results of Chelikowsky and Cohen[31] one can find good correspondence with our calculation not only for the band gaps but also for the conduction bands (see Figs. 7—12). Again, one can notice (cf, Figs. 1—6 and Table II) that our tight-binding parameters provide a much better fit than the other second-neighbor calculations fitted to the same pseudopotential data. It is also fair to mention that with the present choice of model, it is rather difficult to produce deep curvature in the conduction bands, however the general shapes are quite similar with their existing pseudopotential counterparts. The use of the model with interactions including third neighbors (as considered by Papaconstontopoulos and Economou[17] for Si) can definitely improve the overhall band structure, especially the conduction bands, provided the detailed energy-band dispersions are known for directions other than the three major ([100], [011], and [111]) directions.

*Permanent address: Department of Physics, University of Allahabad, Allahabad-211002, India

[1]A. G. Milnes, *Deep Impurities in Semiconductors* (Wiley, New York, 1973), and references cited therein.

[2]A. M. Stoneham, *Theory of Defects in Solids* (Clarendon, Oxford, 1975).

[3]S. T. Pantelides, Rev. Mod. Phys. 50, 797 (1978).

[4]M. Jaros, Adv. Phys. 29, 409 (1980).

[5]J. W. Carbett, J. C. Bourgoin, and C. Weigel, in *Radiation Damage and Defects in Semiconductors,* edited by J. E. Whitehouse Institute of Physics, London, 1972), p. 1.

[6]C. Weigel, D. Peak, J. W. Corbett, G. D. Watkins, and R. P. Messmer, Phys. Rev. B 8, 2907 (1973).

[7]G. D. Watkins and R. P. Messmer, *Computational Methods for Large Molecules and Localized States in Solids,* edited by F. Herman, A. D. McLean, and R. K. Nesbet (Plenum, New York, 1973), p. 133.

[8](a) A. Fazzio, J. R. Leite, and M. L. DeSiqueira J. Phys. C 12, 3469 (1979); (b) L. M. Brescansin and A. Fazzio, Phys. Status Solidi B 105, 339 (1981).

[9]R. P. Messmer and G. D. Watkins, Phys. Rev. B 7, 2568 (1973).

[10]G. B. Bachelet, G. A. Baraff, and M. Schlüter, in Proceedings of AIP Meeting, Phoenix , Arizona, 1981; Phys. Rev. B 24, 943 (1981).

[11]J. Callaway, J. Math. Phys. (N.Y.) 5, 783 (1964); Phys. Rev. 154, 515 (1967); J. Callaway and A. Hughes, *ibid.* 156, 860 (1967); 1043 (1967).

[12](a) M. Jaros and S. Brand, Phys. Rev. B 14, 4494 (1976); (b) M. Jaros and G. P. Srivastva, J. Phys. Chem. Solids 38, 1399 (1977); (c) G. P. Srivastva, Phys. Status Solidi B 93, 761 (1980).

[13]E. Kauffer, P. Pechur, and M. Gerl, J. Phys. C 9, 2319 (1977); Phys. Rev. B 14, 4521 (1976).

[14]J. Bernholc and S. T. Pantelides, Phys. Rev. B 10, 1780 (1978).

[15]H. P. Hjalmarson, P. Vögl, D. J. Wolford, and J. D. Dow, Phys. Rev. Lett. 44, 810 (1980).

[16]A. Madhukar and S. Das Sarma, J. Vac. Sci. Technol.

1, 1120 (1980).
[17]D. A. Papaconstantopoulos and E. N. Economou, Phys. Rev. B 22, 2903 (1980).
[18]S. G. Louie, M. Schlüter, J. R. Chelikowsky, and M. L. Cohen, Phys. Rev. 13, 1654 (1976).
[19]G. A. Baraff, E. O. Kane, and M. Schlüter, Phys. Rev. Lett. 43, 956 (1979).
[20]N. O. Lipari, J. Bernholc, and S. T. Pantelides, Phys. Rev. Lett. 43, 1354 (1979); Phys. Rev. B 21, 3545 (1980).
[21]M. Scheffler, S. T. Pantelides, N. O. Lipari, and J. Bernholc, Phys. Rev. Lett. 47, 413 (1981).
[22]G. F. Koster and J. C. Slater, Phys. Rev. 95, 1167 (1954).
[23]M. Lannoo and P. Lenglart, J. Phys. Chem. Solids 30, 2409 (1969).
[24]K. C. Pandey and J. C. Phillips, Phys. Rev. Lett. 32, 1433 (1974); Phys. Rev. B 13, 750 (1976).
[25]J. B. Krieger and P. M. Laufer, Phys. Rev. B 23, 4063 (1981).
[26]J. Pollman and S. T. Pantelides, Phys. Rev. B 18, 5524 (1978); J. Pollman, in *Festköerperprobleme (Advances in Solid State Physics),* edited by J. Treusch (Vieweg, Braunshweig, 1980), Vol. XX, p. 117.
[27](a) D. J. Chadi and M. L. Cohen, Phys. Status Solidi B 68, 405 (1975). We have noticed that there were some misprints in this paper, especially in defining the (8×8) interaction matrix which have been overlooked in Ref. (39) (see Appendix for correct expression); (b) D. J. Chadi, Phys. Rev. B 16, 790 (1977).
[28]G. C. Osbourn and D. L. Smith, Phys. Rev. B 19, 2124 (1979).
[29]J. N. Schulman and T. C. McGill, Solid State Commun. 34, 29 (1980); J. Vac. Sci. Technol. 17, 1118 (1980); Phys. Rev. B 19, 6341 (1979).
[30]R. N. Nucho and A. Madhukar, J. Vac. Sci. Technol. 15, 1530 (1978).
[31]J. R. Chelikowsky and M. L. Cohen, Phys. Rev. B 14, 556 (1976).
[32]E. Hess, I. Topol, K. R. Schülze, H. Neumann, and K. Unger, Phys. Status Solidi B 55, 187 (1973).
[33]D. J. Stukel and R. N. Euwema, Phys. Rev. 188, 1193 (1969).
[34]P. W. Chye, I. Lindau, P. Pianetta, C. M. Garner, C. Y. Su, and W. E. Spicer, Phys. Rev. B 18, 5545 (1978).
[35]J. S. Best, Appl. Phys. Lett. 34, 522 (1979).
[36]T. F. Keuch and J. O. McCaldin, J. Vac. Sci. Technol. 17, 891 (1980).
[37]M. S. Daw and D. L. Smith, J. Vac. Sci. Technol., 17, 1028 (1980); Appl. Phys. Lett. 36, 690 (1980); Solid State Commun. 37, 205 (1981).
[38]P. J. Lin-Chung and T. L. Reinecke, Solid State Commun. (in press).
[39]W. A. Harrison in *Electronic Structure and the Properties of Solids* (Freeman, San Francisco, 1980).
[40]J. Fischer-Hjalmars, J. Chem. Phys. 42, 1962 (1965).
[41]G. Dresselhaus and M. Dresselhaus, Phys. Rev. 160, 649 (1967).
[42]U. Kaufmann, J. Schneider, and R. Raüber, Appl. Phys. Letts. 29, 319 (1976); U. Kaufmann and J. Schneider, Festköerperprobleme 20, 87 (1980).
[43]R. J. Wagner, J. J. Krebs, and G. H. Stauss, Solid State Commun. 36, 15 (1980).
[44]T. A. Kennedy and N. D. Wilsey, Phys. Rev. Lett. 41, 977 (1978); Phys. Rev. B 23, 6585 (1981).
[45]H. Temkin, B. V. Dutt, and W. A. Bonner, Appl. Phys. Lett. 38, 431 (1981).
[46]J. C. Phillips, in *Bonds and Bands in Semiconductors* (Academic, New York, 1973).
[47]V. Montgomery, A. McKinley, and R. H. Williams, Surf. Sci. 89, 635 (1979).
[48]T. P. Humphreys, M. H. Patterson, and R. H. Williams, J. Vac. Sci. Technol. 17, 886 (1980).
[49]J. O. McCaldin, T. C. McGill, and C. A. Mead, J. Vac. Sci. Technol. 13, 801 (1976).
[50]W. E. Spicer, I. Lindau, P. Skeath, and C. Y. Su, J. Vac. Sci. Technol. 17, 1019 (1980).
[51]K. Kajiyama, Y. Mizushima, and S. Skata, Appl. Phys. Lett. 23, 458 (1973).
[52]L. Ley, R. A. Pollak, F. R. McFeely, S. P. Kawalczyk, and D. A. Shirley, Phys. Rev. B 9, 600 (1974).
[53]G. D. Watkins, in *Defects and Radiation Damage in Semiconductors, 1972,* edited by J. E. White (Institute of Physics, London, 1973), p. 228.
[54]D. V. Lang, R. A. Logan, and L. C. Kimerling, Phys. Rev. B 15, 4874 (1977).
[55]R. H. Wallis, A. Zylbersztejn, and J. M. Besson, Appl. Phys. Lett. 38, 698 (1981).
[56]V. Bartolani, C. Calandra, and M. J. Kelly, J. Phys. C. 6, L349 (1973).